8. Physical Properties of Near-Surface Sediments at Southern Hydrate Ridge: Results from ODP Leg 204[1]

M. Riedel,[2,3] P. Long,[4] C.S. Liu,[5] P. Schultheiss,[6] T. Collett,[7] and ODP Leg 204 Shipboard Scientific Party

ABSTRACT

At the Leg 204 sites located on southern Hydrate Ridge, offshore the Oregon margin, detailed measurements of physical properties in the upper 10–20 m were carried out to characterize the physical nature of the near-surface sediments. Measurements included *P*-wave velocity, magnetic susceptibility, density, porosity, electrical resistivity, and shear strength. At Sites 1244, 1245, and 1246, *P*-wave velocity was also determined on the split cores using the Hamilton frame. Electrical resistivity was measured with the new noncontact resistivity tool from Geotek on whole cores as part of multisensor track core logging at Sites 1244, 1245, 1246, 1247, 1248, and 1252. These data were then used to calculate porosity using moisture and density measurements to develop appropriate transfer functions by using Archie's relation. This data set is important because only limited reliable logging data were obtained in the upper 10–20 m as a result of poor borehole conditions. Sediment porosities appear to be highest at Sites 1251 and 1252 in the slope basin, with values of ~75% in the upper 5 m below seafloor. Porosity is generally ~10% lower at all other sites. Porosity profiles were compared with *P*-wave velocity and sediment shear strength. Apparent overconsolidation of near-surface sediments was observed at Sites 1244, 1245, and 1246. At Site 1251, no such overconsolidation is observed. Sites 1244, 1245, and 1246 are located on the flanks of the anticline at southern Hydrate Ridge and have probably been exposed to erosion, whereas Sites 1251 and 1252, which are located in the eastward basin, have a

much higher recent sedimentation rate as a result of turbidite deposition.

INTRODUCTION

Scientific research coring associated with Leg 204 at southern Hydrate Ridge offshore the Oregon margin focused on the determination of distribution and concentration of gas hydrate in an accretionary ridge and adjacent slope basin (Tréhu, Bohrmann, Rack, Torres, et al., 2003). Main research topics addressed during Leg 204 included the mechanisms of fluid transport (methane and other gases) into the gas hydrate stability zone (GHSZ), the relationship between the stratigraphic and structural setting at southern Hydrate Ridge and the distribution and concentration of gas hydrate, and constraints on physical properties of gas hydrate–bearing sediments.

A suite of physical property measurements was made to compliment the other data measured on board and to support the main scientific objectives of Leg 204. Physical characteristics of the subsurface sediments play an important role in determining the nature of fluid and gas migration, which in turn affects the nature of microbial communities and gas hydrate formation.

In this paper we describe results from analyses focused on the near-surface sediments in the upper 10–20 meters below seafloor (mbsf). This interval is often difficult to cover with logging tools because of hole instabilities, and physical property measurements from logging are therefore often unreliable or unavailable.

We also present data acquired with the newly developed Geotek non-contact resistivity (NCR) tool. Historically, resistivity measurements during Ocean Drilling Program (ODP) legs were carried out on split cores using a four-pin Wenner electrode array, and results were affected by the splitting process as well as moisture loss resulting from continuous exposure of the sediments in addition to gas expansion cracks. The NCR tool measures resistivity before splitting and therefore avoids artifacts caused by splitting and allows a direct correlation with the other components of the multisensor track (MST; such as *P*-wave velocity, gamma ray attenuation [GRA] density, and magnetic susceptibility).

Porosity and sediment shear strength measurements also are important indicators of seafloor stability. Analyses of density and *P*-wave velocity yield estimates of seafloor impedance, which can subsequently be used to calibrate points in seismic studies of seafloor reflection coefficients. The analyses shown here cover the upper 10 mbsf and therefore allow characterization of the physical properties of those sediments on a seismic scale (for typical marine seismic survey frequencies of ~100 Hz).

METHODS

After sectioning the core on the catwalk, the core sections were stored inside the laboratory and allowed to equilibrate to ambient room temperature (~4 hr). After temperature equilibration, bulk sediment physical properties were measured using the MST on whole-round cores. Measurements included NCR, compressional wave velocity, GRA bulk density, and magnetic susceptibility. The core sections were then split for discrete sampling for moisture and density (MAD) and for mea-

surements of shear strength (using the automated shear vane [ASV] and a handheld Torvane) and compressional wave velocity using a Hamilton frame velocimeter using three different directions of wave propagation: x-component (*P*-wave sensor [PWS]-1), y-component (PWS2), and z-component (PWS3).

For details about the standard ODP physical property sensors and laboratory techniques (MAD, GRA, magnetic susceptibility, compressional wave velocity, and shear strength), see the "Explanatory Notes" chapter in the Leg 204 *Initial Reports* volume (Tréhu, Bohrmann, Rack, Torres, et al., 2003) and Blum (1997).

The Geotek NCR system operates by inducing a high-frequency magnetic field in the core from a transmitter coil, which in turn induces electrical currents in the core, which are inversely proportional to the resistivity. A receiver coil measures the magnetic field generated by the electrical current. To measure these very small magnetic fields accurately, the readings generated from the measuring coils are compared to the readings from an identical set of coils operating in air. This technique provides the required accuracy and stability. Resistivities between 0.1 and 10 Ωm can be measured at ~2- to 4-cm spatial resolutions along the core. As with other parameters, the measurements vary with core temperature and should be obtained in a stable temperature environment for best results.

The NCR system was calibrated with standards consisting of short lengths of core liner (~25 cm) filled with water of known NaCl concentrations. The core logging results are illustrated in Figure **F1A,** which shows the raw output data in millivolts decreasing with decreasing salinity. The drop in output between the calibration sections illustrates the effect of having electrical insulating gaps between the samples. Averaged values at each salinity concentration are then plotted against the theoretical resistivity in Figure **F1B,** which provides a power-law calibration equation. This calibration equation is only valid for measurements taken at Sites 1244 (Hole 1244E), 1245, 1246, 1247, 1248, 1249, 1250, and 1252. All other measurements were conducted without calibration and are disregarded in this study.

The NCR is very sensitive to gas cracks or voids (acting as electrical insulators), which result in highly variable measurements in gassy sediments. Most of the cores recovered during Leg 204 from within the gas hydrate occurrence zone suffered significant disturbance caused by gas expansion effects. Expansion of free gas, exsolution of dissolved gas, and dissociation of gas hydrate contributed to the gas expansion effect during Leg 204. When relatively small volumes of gas exsolve from pore fluids during core recovery, bubbles form in the sediment matrix with only minor amounts of core volume expansion. As the gas volumes become greater, the sediment structure begins to fracture and the cores expand, forming a series of large gas voids in the core. When core expansion occurs, the core is generally pushed back together prior to sectioning, but inevitably these fractures remain in the core and affect physical property measurements. The pervasive nature of gas expansion is illustrated in Figure **F2,** which shows an image of an advanced piston corer section through the liner before it was split. (Section 204-1251G-1H-5; 8.5–10 mbsf).

The effect of mechanically pushing together the sediments in the liner and the pervasive expansion cracks on the measured physical properties is difficult to estimate and quantify. In this paper we focus on the upper 10–20 mbsf, which generally did not suffer significantly from gas expansion and did not require mechanical pushing to close voids. If

F1. NCR calibration, p. 14.

F2. Gas expansion cracks, p. 15.
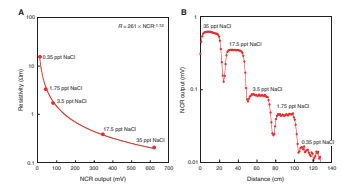
gas expansion was present and the sediments showed cracking on the split core, we generally avoided those sections to measure *P*-wave velocity and shear strength. These sections are also clearly identifiable on the MST records by an increase in the scatter of GRA density and NCR values and are therefore excluded from the detailed discussion. The MAD analyses are probably not affected significantly since the combination of measuring weight and volume before and after drying of a sample is believed to account for extra (artificial) voids from gas expansion that would artificially increase porosity. The general good agreement between GRA, MAD, and independent logging estimates from wireline logging and logging while drilling shows that our assumptions are valid (see the "Physical Properties" sections in the individual site chapters in the Leg 204 *Initial Results* volume; Tréhu, Bohrmann, Rack, Torres, et al., 2003).

RESULTS

At Sites 1244, 1245, and 1246, a complete set of physical property measurements was acquired in the upper 10 m of sediments. At Sites 1247 and 1248, only limited NCR data are available, which can be compared to MAD results. Because of the extreme gas expansion, velocity and shear strength also could not be determined. A key item in this analysis is the estimation of porosity. There are several ways of calculating porosity using (1) density from the MAD samples, (2) NCR, and (3) GRA densities. The MAD data directly yield porosities by comparing wet and dry mass for a known volume of sediment (see Blum, 1997). Porosity (Φ) and density (ρ_b) are related by the following equation using grain density ρ_g and pore water density ρ_w:

$$\Phi = (\rho_g - \rho_b)/(\rho_g - \rho_w).$$

Grain density was determined by MAD analyses and was, on average, 2.7 g/cm³. Pore water density was assumed to be 1.05 g/cm³.

The available NCR data that correspond to a MAD data point were used to relate MAD-derived porosity to NCR porosity. NCR was first used to calculate formation factor (FF). Formation factor is defined as the ratio between the measured resistivity of the core and the resistivity of the pore water. To do this, a resistivity of 0.21739 Ωm for standard seawater (assumed salinity of near-surface sediments) at a room temperature of 20°C was used. The NCR measurements were carried out at about the same temperature as the standards, and no additional temperature correction was needed. There are only ~90 data points from the near-surface sediment interval to constrain this relation (Fig. F3), but these porosity estimates are generally in good agreement with porosities determined from the GRA density records.

Our data for the near-surface sediments (0–20 mbsf) yield a relation between FF and MAD porosity after Archie's relation in the form of

$$FF = a\Phi^{-m},$$

with the best-fit Archie parameters $a = 1.684$ (tortuosity) and $m = 1.267$ (cementation). They are, however, significantly different from previously reported values from ODP Legs 146 ($a = 1.41$, $m = 1.76$; Westbrook,

F3. Formation factor and porosity, p. 16.
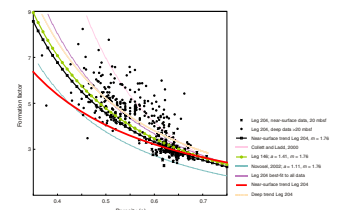
Carson, Musgrave, et al., 1994) and 164 (*a* = 1.0, *m* = 2.8; Collett and Ladd, 2000).

The cementation coefficient is characteristic to a given rock type. If the Archie relation is chosen to be consistent with results from Leg 146 Site 892 (northern Hydrate Ridge) and constraining *m* to 1.76, the best-fit tortuosity coefficient is 1.35 for the near-surface sediments. The difference between these two sets of Archie parameters is considered negligible, and we therefore decided to use a set of Archie parameters that is consistent with the earlier data and use the values *a* = 1.35 and *m* = 1.76 for near-surface sediments (shallower than 20 mbsf).

If data from depths below 20 mbsf are considered in the Archie relation, the above relation is unable to explain the observed trend. A best power-law fit to the entire data range for all depths yields the Archie coefficients *a* = 1.37 and *m* = 1.93. Restricting the range of data to only sediments deeper than 20 mbsf yields *a* = 1.575 and *m* = 1.73. However, both of these functions are not appropriate for the near-surface sediments because they predict porosities that are too high. The near-surface trend in turn predicts porosities that are too low for depths below 20 mbsf.

Two alternative sets of Archie parameters may be considered. The relation by Collett and Ladd (2000), with *a* = 1.0 and *m* = 2.8, predicts porosities that are well above the observed trend of Leg 204 and are unsuitable for this study (Fig. F3). In a recent study of piston cores taken from the northern Cascadia margin around an active cold vent near ODP Site 889, Novosel (2002) showed that the best-fit Archie parameters for those near-surface sediments shallower than 10 mbsf are *a* = 1.1 and *m* = 1.76. This predicts porosities that are much lower than what is observed at southern Hydrate Ridge. Novosel (2002) concludes that the near-surface sediments cannot be described with the same Archie parameters as defined from the entire Site 889 core data and that a separate parameter set is required for the near-surface sediments. Similarly, it appears that there is no universal function for the entire Leg 204 data set (i.e., near-surface sediments have to be treated separately from the deeper sediments).

In the following site-by-site review of the results, we compare porosities derived directly through MAD analysis, density porosity using GRA data, and porosities derived from NCR data using Archie parameters *a* = 1.35 and *m* = 1.76.

Site 1244

At Site 1244, a complete NCR record was measured only for Hole 1244E. These data are compared to other physical property measurements from Holes 1244A, 1244B, 1244C, and 1244D (Fig. F4). Individual holes are ~40–50 m apart, but physical properties were assumed not to vary significantly because this site is not located at the summit of Hydrate Ridge, where the sediments host extremely high gas hydrate concentrations in the upper 50 mbsf and show strong lateral variability.

P-wave velocity measured with the MST increases linearly from ~1480 m/s near the seafloor (shallower than 2 mbsf) to ~1550 m/s at 8 mbsf. Velocities measured on the split core from Hole 1244E are ~20–30 m/s higher than the MST results. The PWS2 velocity, measured along the y-plane, was consistently higher by ~25 m/s than in the x- and z-directions. Figure F4E shows that shear strength increases linearly with depth from 20 kPa in the upper 1 mbsf to ~60 kPa at 8 mbsf. The GRA density profile shows very low densities of 1.45 g /cm³ in the upper 1

F4. Physical properties, Site 1244, p. 17.
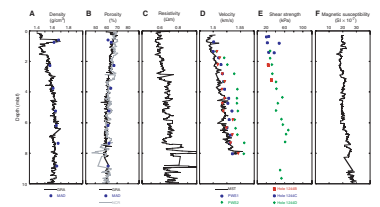
mbsf and increases to ~1.6 g/cm³ at 6 mbsf. Below 6 mbsf, density remains relatively constant at ~1.6 g/cm³. Porosities derived from MAD, GRA density, and NCR are similar and decrease downcore from values of ~70% at the seafloor to ~60% at 8 mbsf. Below 7 mbsf the NCR record is more variable, which is related to the beginning of gas expansion crack formation.

Site 1245

Results from Site 1245 are summarized for Holes 1245B and 1245C (Fig. F5). In general, results from Site 1245 are similar to those from Site 1244. Shear strength increases linearly with depth from 20 kPa at the seafloor to 80–100 kPa at 10 mbsf. *P*-wave velocity, measured with the MST only between 1.8 and 8 mbsf, is generally above 1500 m/s and increases linearly with depth. The data points from the split core analyses show a general trend to slightly higher values compared to the MST measurements. Velocity values deeper than 7.5 mbsf range widely between 1475 and 1585 m/s, which may be the result of gas expansion cracks limiting the accuracy in the velocity measurements.

Measured bulk densities are relatively constant with values of ~1.7 g/cm³. Porosities derived from MAD, NCR, and GRA density generally agree, but there are several consistent differences. Porosities from GRA and NCR are both very low in the upper 0.5 mbsf, with values as low as 55%. NCR and GRA porosities increase below this upper 0.5-m-thick layer and are similar to the MAD results from shallower than 1.5 mbsf. NCR porosity is then much higher than MAD and GRA porosity until a sudden drop in NCR porosity is seen at 4.5 mbsf. For the remainder of the entire interval investigated, MAD and GRA porosities agree, but NCR porosity is slightly higher. The NCR profile, however, reveals fine-scale variations similar to the GRA record. Below 8 mbsf, NCR and GRA show influence of developing gas expansion cracks.
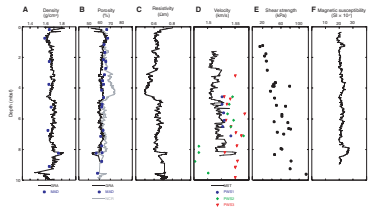
Site 1246

At Site 1246, only five AVS shear strength measurements could be carried out. All remaining measurements were carried out with the handheld Torvane. Values increase linearly to ~60 kPa at 8 mbsf. Figure F6 compares all measured physical properties at this site. *P*-wave velocity was measured with the MST for the upper 4.5 mbsf. Velocities from the split cores are again higher than the MST results. *P*-wave velocity remains almost constant in the upper 6 mbsf and then increases with depth as seen in the split-core data. Two layers show velocity increases in the MST record at ~1.0 and 3.8 mbsf, which are also seen in the GRA density profile, with densities as high as 1.75 g/cm³ relative to the surrounding densities of 1.65 g/cm³. Both layers are also characterized by reduced NCR and GRA porosities.
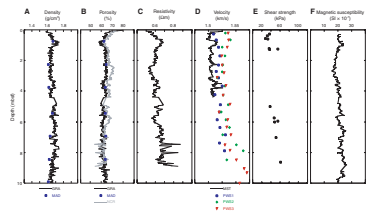
Sites 1247 and 1248

Sites 1247 and 1248 were drilled along a north–south transect between Site 1245 and the summit of southern Hydrate Ridge. Site 1248 is situated an area with increased seafloor acoustic backscatter, which was correlated to carbonate formations (Tréhu, Bohrmann, Rack, Torres, et al., 2003). Velocity and shear strength measurements were not conducted at either site; however, NCR data were acquired and are compared to the GRA and MAD data (Fig. F7). At Site 1247, NCR data start
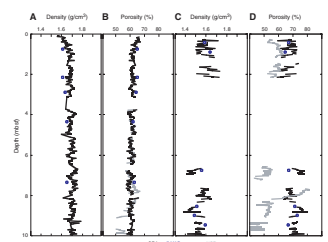
F5. Physical properties, Site 1245, p. 18.

F6. Physical properties, Site 1246, p. 19.

F7. Physical properties, Sites 1247 and 1248, p. 20.

below 3.5 mbsf and agree with the corresponding MAD and GRA de-
rived porosities (Fig. F7B). Porosity decreases from 65% at the seafloor
to ~60% at 10 mbsf. Core recovery at Site 1248 was poor in the up-
per 10 mbsf, with only four sections available for measurements. In the up-
per 1.0 mbsf, MAD, GRA, and NCR porosities show similar values of
~65%, whereas below 6 mbsf, the NCR data are lower than the MAD es-
timates by ~10% and are also extremely scattered as a result of gas ex-
pansion cracks.

Site 1252

Site 1252 is located in the eastern slope basin along a main east–west
transect of core holes. At this site, velocity and shear strength measure-
ments were not made because of the poor quality of the recovered
cores. NCR data were measured in the upper 4 mbsf only. Below 4.0
mbsf, core samples were strongly affected by gas expansion cracks.
NCR, GRA, and MAD porosities at this site show very high values to
80% in the upper 1.0 mbsf (Fig. F8). Porosities decrease significantly
within the upper 2 mbsf and remain constant to 8 mbsf before they
start to increase again. These very high porosities in the shallow subsea-
floor interval were only observed at Sites 1252 and 1251 (no NCR data).

GENERAL CORRELATIONS
BETWEEN PROPERTIES

Porosity data from the NCR system were correlated with shear
strength, density, and *P*-wave velocity for corresponding depth inter-
vals (Fig. F9). There is an apparent correlation between shear strength
and porosity or density, although the corresponding R^2 values for a lin-
ear regression are <0.35 (Fig. F9C, F9D). GRA density and MST *P*-wave
velocity show a well-defined, almost linear correlation, as also reported
by Hamilton and Bachmann (1982) and Hamilton (1980) (Fig. F9B).

Shear strength increased linearly with depth in the upper 10 mbsf,
whereas porosity and density remained relatively constant over the
equivalent depth ranges. Shear strength is, however, linearly correlated
with *P*-wave velocity at Sites 1244, 1245, and 1246. The linear relation-
ship is better shown if the different types of measurements (MST or
split-core analyses with PWS1, PWS2, and PWS3 sensors) are considered
separately (Fig. F10). A plot of all velocity/shear strength pairs does not
show a strong correlation. A number of anomalous velocity values were
acquired with the PWS3 sensor at Site 1246 (Fig. F10E). Results for this
site differ from the otherwise well-developed linear trend. These data
were acquired at a greater subbottom depth below 8 mbsf, where alter-
ation by gas expansion cracks was greater (cf. Fig. F6D).

Porosity and *P*-wave velocity show a strong correlation (Fig. F9A).
The derived relation is in good agreement with results from shallow pis-
ton cores from the northern Cascadia margin near the location of Site
889 (Novosel, 2002) but is significantly different from other published
trends (Hyndman et al., 1993; Jarrad et al., 1995) that predict higher ve-
locities for the same porosity values. The study by Hyndman et al.
(1993) was derived from sediments with porosities <60%, whereas the
sediments in this study generally have much higher porosities. The
study by Jarrad et al. (1995) using Site 889 combines both shallow and
deeper sediments and is considered valid for porosities as high as 80%.
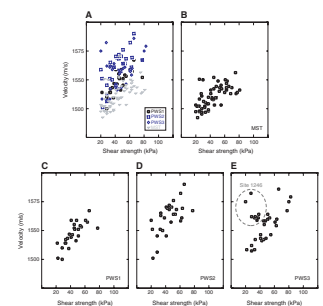
F8. Physical properties, Site 1252,
p. 21.
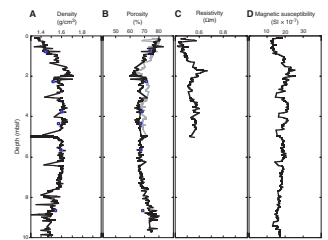
F9. Porosity and velocity, p. 22.
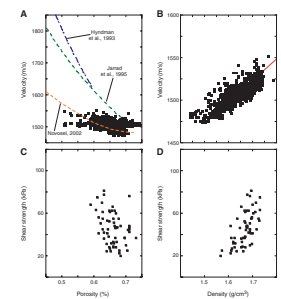
F10. Velocity and shear strength,
p. 23.

DOWNCORE IMPEDANCE AND
REFLECTION COEFFICIENTS

Seismic impedance, the product of sediment bulk density and seismic velocity, was calculated downcore at Sites 1244, 1245, and 1246 using GRA-derived bulk density and MST velocity (Fig. F11). At Site 1245, measurements are restricted to a depth range of 1.6–8.5 mbsf, whereas at Site 1246, impedance could be calculated only to a total depth of 4.6 mbsf.

Seismic impedance in the upper 1.0 mbsf is significantly larger at Site 1246 than at Site 1244 but is almost identical over the depth range of 1.0–4.0 mbsf. Below 4.0 mbsf, seismic impedance at Sites 1244 and 1245 appears relatively constant.

The values of seismic impedance (I) were used to calculate seismic reflection coefficients (RC) of the seafloor using a density of 1035 kg/m^3 and a seismic velocity of 1485 m/s for the water column properties using the following equation:

$$RC = (I_{sed} - I_{water})/(I_{sed} + I_{water}).$$

Reflection coefficients were calculated over depth ranges averaging 1.0, 2.0, 4.0, and 8.0 mbsf (Table T1). At Site 1246, the reflection coefficient decreases with increasing depth range as a result of very high impedance values in the upper 1.0 mbsf, whereas at the other two sites, reflection coefficient increases with the depth range used.

These reflection coefficients can be used to calibrate seismic reflection amplitudes; however, the reflection coefficient is dependent on the frequency spectrum used in the seismic survey. The lower the seismic frequency, the lower the resolution, and the seismic amplitudes reflect physical properties averaged over a larger depth range. A typical rule of thumb to calculate the resolution limit of seismic data is to use one-quarter of the wavelength (l), where the wavelength is given as a function of velocity (c) and frequency (f) by the following relation:
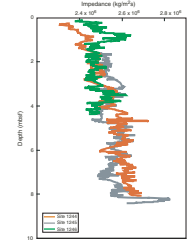
$$c = l \times f.$$

In order to resolve a layer of 1.0 m thickness (wavelength = 4 m) for an average seismic velocity of 1500 m/s, a frequency as high as 380 Hz must be used (Table T1). Whereas most offshore seismic surveys are carried out with much lower frequencies (<100 Hz), the resolution limit of these surveys is <4.0 m. It is therefore important to estimate the reflection coefficient from physical property measurements over a greater depth range.

APPARENT OVERCONSOLIDATION

The ratio of shear strength to overburden pressure is a measure of the consolidation state of sediments. If the ratio is 0.25, the sediment is normally consolidated for its burial depth. The sediment is defined as underconsolidated if the ratio is <0.25 and overconsolidated if the ratio is >0.25. Sediments in the upper 5–10 mbsf often show what is called apparent overconsolidation (AOC; i.e., the ratio of shear strength to overburden is >0.25, often with values as high as 10). This abnormally high ratio can often be an artifact if the sediments have not been care-

fully handled or if the overburden pressure is incorrectly calculated (e.g., using a wrong mudline definition). The ratio of shear strength to overburden is also strongly affected by biogenic components in the sediment, clay mineralogy, age, sedimentation rate, erosion, and cementation (e.g., Silva and Jordan, 1984; Nacci et al., 1974; Skempton, 1970; Francisca et al., 2005).

We observed AOC at Sites 1244, 1245, and 1246 within the upper 10–40 mbsf (Fig. F12A, F12B, F12C). However, at Site 1251 no such AOC was observed (Fig. F12D).

Since we can exclude incorrect mudline definition and improper sediment treatment, the observed AOC is believed to be a real property of the sediments.

AOC is only observed at Sites 1244, 1245, and 1246, and there is no obvious correlation with the occurrence of carbonate cementation (increase in shear strength), biogenic opal (decrease in shear strength), and grain-size distribution within the upper 40 mbsf (see "Lithostratigraphy" sections in the Sites 1244, 1245, and 1246 chapters in the Leg 204 *Initial Results* volume; Tréhu, Bohrmann, Rack, Torres, et al., 2003). AOC at Site 1246 is about twice that at Sites 1244 and 1245. However, all three sites with AOC are located at the flank of the southern Hydrate Ridge anticline and therefore have most likely been shut off from recent and more rapid sedimentation by turbidites. Furthermore, these three sites were probably affected by erosion as part of the uplift of the anticline. The removal of overburden pressure by erosion in combination with a slow pelagic sedimentation rate can explain the observed AOC.

No AOC is observed at Site 1251. This site is located in a basin east of the anticline of southern Hydrate Ridge and is probably prone to a large supply of sediments through turbidite sedimentation and almost no erosion. Site 1251 has the highest sedimentation rate (160 cm/k.y. in the upper 100 mbsf) of all of the sites analyzed during Leg 204. This site is also characterized by an increased concentration of biogenic opal in the upper 20 mbsf, which also decreases shear strength and, therefore, AOC.

ABNORMALLY HIGH NEAR-SURFACE POROSITIES AT THE BASIN SITES

The porosity of sediments gradually decreases with depth as a result of compaction. This phenomenon can be described by Athy's (1930) relation

$$\phi = \phi_0 e^{-Z/L},$$

where ϕ_0 is the surface sediment porosity, Z is the depth, and L is the characteristic decay constant. We used the MAD-derived porosities at Sites 1244, 1245, 1246, 1251, and 1252 for this analysis only. As seen in Figure F13, the porosity generally decreases at all sites with depth following Athy's relation. This general decreasing trend is overprinted by structurally controlled porosity anomalies associated with Horizons A, B, and Y (Riedel et al., 2003). We calculated the decay constant L using Athy's relation for the entire sediment column, avoiding the structural anomalies of Horizons A, B, and Y (Table T2). The upper 5–10 mbsf at Sites 1251 and 1252 and, to a lesser degree, at Sites 1244 and 1245, however, show higher porosities than are predicted from the deeper trend using Athy's

F12. Shear strength and pressure ratio, p. 25.
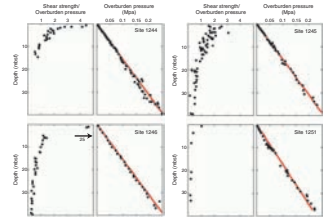
F13. Downcore porosity, p. 26.
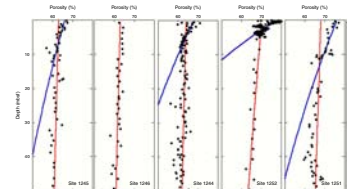
T2. Age of events, p. 28.

law. This phenomenon is absent at Sites 1246, 1247, 1248, 1249, and 1250. It should be noted that poor core recovery at Sites 1248, 1249, and 1250 may bias the observation.

Using the upper 5–10 mbsf at Sites 1244, 1245, 1251, and 1252, a different set of decay constants was calculated for these sites (Table T2). The decay constant L is about one order of magnitude smaller, reflecting the rapid compaction rate (or dewatering) of those near-surface sediments. The difference between anticline-flank Sites 1244 and 1245 and basin Sites 1251 and 1252 is mainly in the surface porosity ϕ_0, which is ~10% higher at the basin sites. An exceptionally small decay constant ($L = 26$) was calculated at Site 1252; however, super-high porosities are only observed in the upper 2 mbsf. The fact that high near-surface porosities are observed at Sites 1244 and 1245 may be the reason why the AOC at these two sites is less pronounced than at Site 1246, which does not show any high near-surface porosities.

Unusually high near-surface porosities have been reported by many authors over the last few decades (e.g., Bennett et al., 1970; Booth and Dahl, 1986; Boudreau, 1998; Novosel, 2002). Physical properties of sediment are not just affected by overburden stress but are also a function of the nature of microfabric, amount of organic matter, and mineralogy, as well as grain size and shape (Bennett et al., 1999). For example, the presence of clays, especially the mineral smectite, can significantly increase the expected porosity and water content within the top few meters of the sediment (e.g., Velde and Espitalie, 1996; Bennett et al., 1999). This phenomenon, often referred to as flocculation, is attributed to the clay's active electrostatic forces that allow "edge-edge" assemblage of the clay platelets, with increased water content filling the voids (Velde, 1996). Flocculation can also result in decreased shear strength (i.e., this type of sediment would show a smaller degree of AOC, as discussed in the previous section).

Biostratigraphic analyses show that sediments at the basin Sites 1251 and 1252 are much younger in the upper 10 mbsf than at all the other Sites (Tréhu, Bohrmann, Rack, Torres, et al., 2003). The youngest microfossils, with an age of ~0.09 Ma, were identified at these two basin sites only at depths below 15 mbsf (Table T3).

SUMMARY AND CONCLUSIONS

Analyses of sediment physical properties during Leg 204 yield useful insight to the nature of the near-surface sediment interval just beneath the seafloor. Using the ODP standard MST core logger with P-wave velocity, GRA density, and magnetic susceptibility together with the newly developed Geotek NCR sensor allowed unique opportunities to compare and correlate in detail different physical properties. It was also the first test of the NCR sensor during an ODP leg.

At Sites 1244, 1245, and 1246, a complete set of physical property data were acquired including MAD samples, MST data, and velocity and shear strength from split-core analyses. At several other sites (1247, 1248, and 1252) only subsets of physical property data could be acquired, limited by gas expansion cracks.

Resistivity data were used to estimate porosity following Archie's relation using the MAD samples as calibration points. The results from this analysis were in good agreement with Leg 146 Site 892 studies. The NCR-derived porosity values agree well with other independent porosity estimates, such as GRA density porosity. NCR data further suggest

T3. Decay constants and porosities, p. 29.

that the resistivity-porosity relation described by Archie's law is different in the near-seafloor sediment section ($a = 1.35$, $m = 1.76$) than within the deeper sediment column ($a = 1.575$, $m = 1.73$), as has also been observed on the northern Cascadia margin. Merging the two different depth ranges and estimating the best-fit Archie parameters for all data ($a = 1.37$, $m = 1.93$) artificially increases the porosity estimates for the near-seafloor sediments. The difference in the estimated Archie parameters has no implications on gas hydrate concentration estimates because the upper 10–20 mbsf did not contain any gas hydrate at the sites considered in this study.

NCR porosity appears well correlated with *P*-wave velocity, but shows a different relation than previously published (e.g., Hyndman et al., 1993; Jarrad et al., 1995). We observed no strong correlation between porosity and shear strength. Overall, *P*-wave velocity appears to uniformly increase with depth at all three sites, ranging from ~1480 m/s at the seafloor to ~1550 m/s at 8–10 mbsf. Shear strength also increases with depth at all sites, from ~20 kPa near the seafloor to 60–80 kPa at 8–10 mbsf, and thus a clear linear correlation is observed between shear strength and *P*-wave velocity.

Downcore seismic impedance and reflection coefficients were calculated at Sites 1244, 1245, and 1246 and can be used to calibrate seismic reflection surveys. However, the frequency content of the seismic data has to be considered in the calibration to account for the depth variation of seismic impedance over the upper 10 mbsf.

From all the analyses it can be concluded that the sediments at the slope basin (Sites 1251 and 1252) have much higher porosity (lower bulk densities) in the upper 10 mbsf than those close to or at the summit of southern Hydrate Ridge associated with low AOC. This may reflect a lower compaction state combined with higher sedimentation rates for the slope basin sites. The other sites located at the flank or on top of Hydrate Ridge may not receive as much sediment (i.e., they are detached from recent Holocene turbidite sedimentation). The observed high state of AOC may also be interpreted as a result of erosion, which may also be indicated by the relatively older age of the near-seafloor sediments at Sites 1244, 1245, and 1246 compared to basin Sites 1251 and 1252.

ACKNOWLEDGMENTS

REFERENCES

Athy, L.F., 1930. Density, porosity, and compaction of sedimentary rocks. *AAPG Bull.,* 14:1–24.

Bennett, R.H., Keller, G.H., and Busby, R.F., 1970. Mass property variability in three closely-spaced deep-sea sediment cores. *J. Sediment. Petrol.,* 40(3):1038–1043.

Bennett, R.H., Ransom, B., Kastner, M., Baerwald, R.J., Hulbert, M.H., Sawyer, W.B., Olsen, H., and Lambert, M.W., 1999. Early diagenesis: impact of organic matter on mass physical properties and processes, California continental margin. *Mar. Geol.,* 159(1–4):7–34. **doi:10.1016/S0025-3227(99)00003-1**

Blum, P., 1997. Physical properties handbook: a guide to the shipboard measurement of physical properties of deep-sea cores. *ODP Tech. Note,* 26 [Online]. Available from World Wide Web: <**http://www-odp.tamu.edu/publications/tnotes/tn26/ INDEX.HTM**>. [Cited 2006-07-10]

Booth, J.S., and Dahl, A.G., 1986. A note on the relationships between organic matter and some geotechnical properties of a marine sediment. *Mar. Geotechnol.,* 6(3):281–297.

Boudreau, B.P., 1998. Mean mixed depth of sediments: the wherefore and the why. *Limnol. Oceanogr.,* 43(3):524–526.

Collett, T.S., and Ladd, J., 2000. Detection of gas hydrate with downhole logs and assessment of gas hydrate concentrations (saturations) and gas volumes on the Blake Ridge with electrical resistivity log data. *In* Paull, C.K., Matsumoto, R., Wallace, P.J., and Dillon, W.P. (Eds.), *Proc. ODP, Sci. Results,* 164: College Station, TX (Ocean Drilling Program), 179–191. [**HTML**]

Francisca, F., Yun, T.-S., Ruppel, C., and Santamarina, J.C., 2005. Geophysical and geotechnical properties of near-seafloor sediments in the northern Gulf of Mexico gas hydrate province. *Earth Plant. Sci. Lett.,* 237(3–4):924–939. **doi:10.1016/ j.epsl.2005.06.050**

Hamilton, E.L., 1980. Geoacoustic modeling of the seafloor. *J. Acoust. Soc. Am.,* 68:1313–1340.

Hamilton, E.L., and Bachman, R.T., 1982. Sound velocity and related properties of marine sediments. *J. Acoust. Soc. Am.,* 72:1891–1904.

Hyndman, R.D., Moore, G.F., and Moran, K., 1993. Velocity, porosity, and pore-fluid loss from the Nankai subduction zone accretionary prism. *In* Hill, I.A., Taira, A., Firth, J.V., et al., *Proc. ODP, Sci. Results,* 131: College Station, TX (Ocean Drilling Program), 211–220.

Jarrard, R.D., MacKay, M.E., Westbrook, G.K., and Screaton, E.J., 1995. Log-based porosity of ODP sites on the Cascadia accretionary prism. *In* Carson, B., Westbrook, G.K., Musgrave, R.J., and Suess, E. (Eds.), *Proc. ODP, Sci. Results,* 146 (Pt 1): College Station, TX (Ocean Drilling Program), 313–335.

Nacci, V.A., Kelly, W.E., Wang, M.C., and Demars, K.R., 1974. Strength and stress-strain characteristics of deep-sea sediments. *In* Inderbitzen, A.L. (Ed.), *Deep-Sea Sediments: Physical and Mechanical Properties: Determination of Mechanical Properties in Marine Sediments.* Mar. Sci. (Plenum), 2:129–150.

Novosel, I., 2002. Physical properties of gas hydrate related sediments, offshore Vancouver Island [M.Sc. Thesis]. Univ. Victoria, Canada.

Riedel, M., Long, P., Liu, C.S., Schultheiss, P., and the ODP Leg 204 Scientific Party, 2003. Ocean Drilling Program (ODP) Leg 204 physical properties: stratigraphic and structural control of hydrate formation [EGS-AGU-EUG Joint Assembly, Nice, 06–11 April 2003].

Silva, A.J., and Jordan, S.A., 1984. Consolidation properties and stress history of some deep sea sediments. *In* Denness, B. (Ed.), *Seabed Mechanics:* London (Graham and Trotman), 25–39.

Skempton, A.W., 1970. First-time slides in over-consolidated clays, technical notes. *Geotechnique,* 20:320–324.

Su, X., Watanabe, M., Trehu, A., Bohrmann, G., Rack, F., and the Leg 204 Shipboard Scientific Party, 2003. Biostratigraphy of late Pliocene to Holocene sediments from southern hydrate ridge, ODP Leg 204 [EGS-AGU-EUG Joint Assembly, Nice, 06–11 April 2003].

Tréhu, A.M., Bohrmann, G., Rack, F.R., Torres, M.E., et al., 2003. *Proc. ODP, Init. Repts.,* 204 [CD-ROM]. Available from: Ocean Drilling Program, Texas A&M University, College Station TX 77845-9547, USA. [**HTML**]

Velde, B., and Espitalie, J., 1989. Comparison of kerogen maturation and illite/smectite composition in diagenesis. *J. Pet. Geol.,* 12(3–4):103–110. **doi:10.1016/0025-3227(96)00020-5**

Westbrook, G.K., Carson, B., Musgrave, R.J., et al., 1994. *Proc. ODP, Init. Repts.,* 146 (Pt. 1): College Station, TX (Ocean Drilling Program).

Figure F1. Calibration of noncontact resistivity (NCR) tool. **A.** Raw measurements of different seawater standards. **B.** Correlation of known seawater resistivity and NCR measurements with best-fit function.
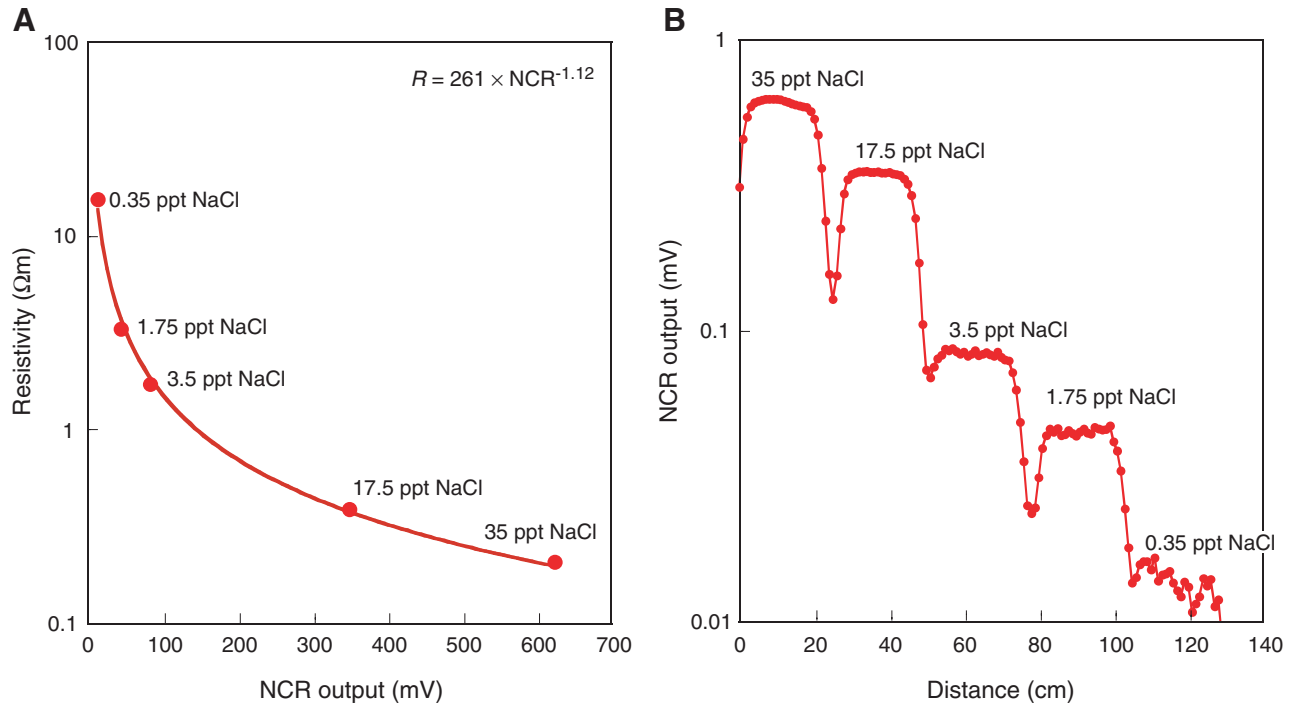

A

$R = 261 \times NCR^{-1.12}$

0.35 ppt NaCl

1.75 ppt NaCl

3.5 ppt NaCl

17.5 ppt NaCl

35 ppt NaCl

Resistivity (Ωm)

NCR output (mV)

B

35 ppt NaCl

17.5 ppt NaCl

3.5 ppt NaCl

1.75 ppt NaCl

0.35 ppt NaCl

NCR output (mV)

Distance (cm)

Figure F2. Gas expansion cracks in sediment core (Section 204-1251G-1H-5; 8.5–10.0 mbsf).
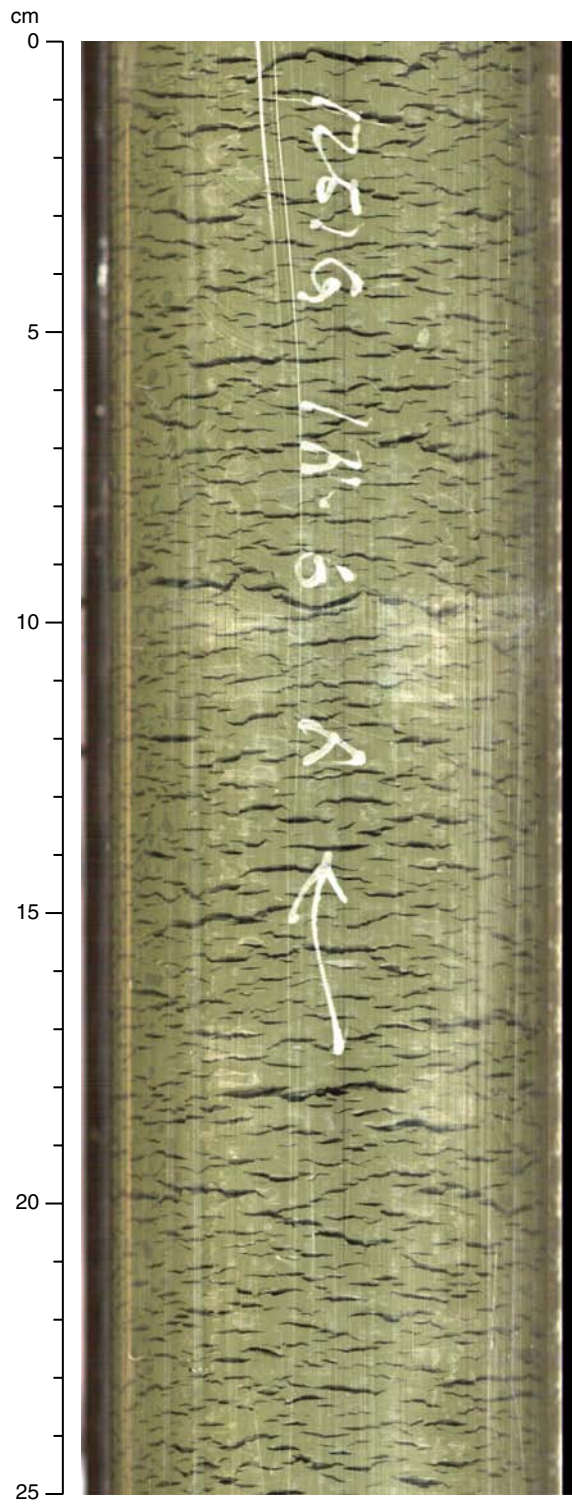
Figure F3. Relation between formation factor and porosity. Shown are several different relations (Archie relation) using data from Legs 146 and 204 (see text for details).
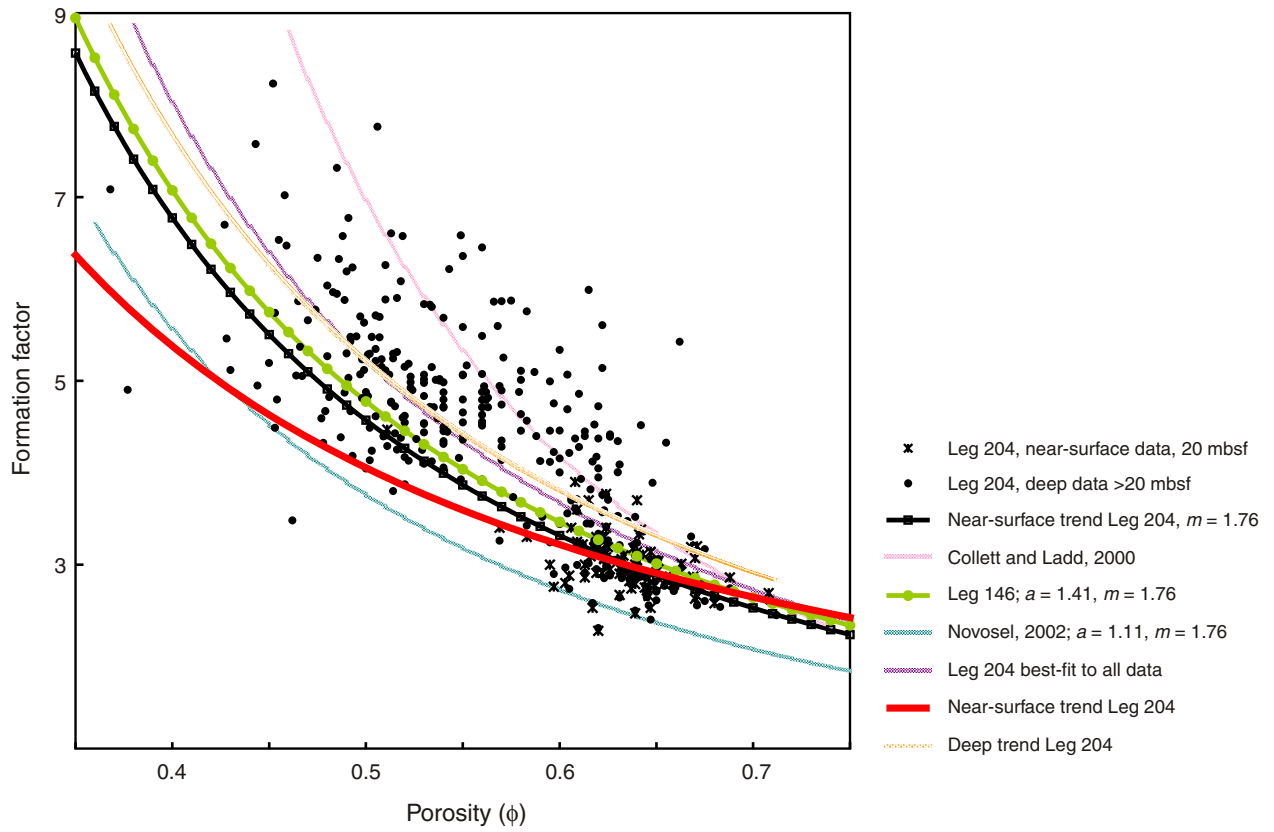
Figure F4. Physical properties of near-surface sediments at Site 1244. **A.** Bulk density. GRA = gamma ray attenuation, MAD = moisture and density. **B.** Porosity. NCR = noncontact resistivity. **C.** Electrical resistivity (NCR). **D.** *P*-wave velocity using multisensor track (MST) and Hamilton frame. PWS = *P*-wave sensor. **E.** Shear strength. **F.** Magnetic susceptibility.
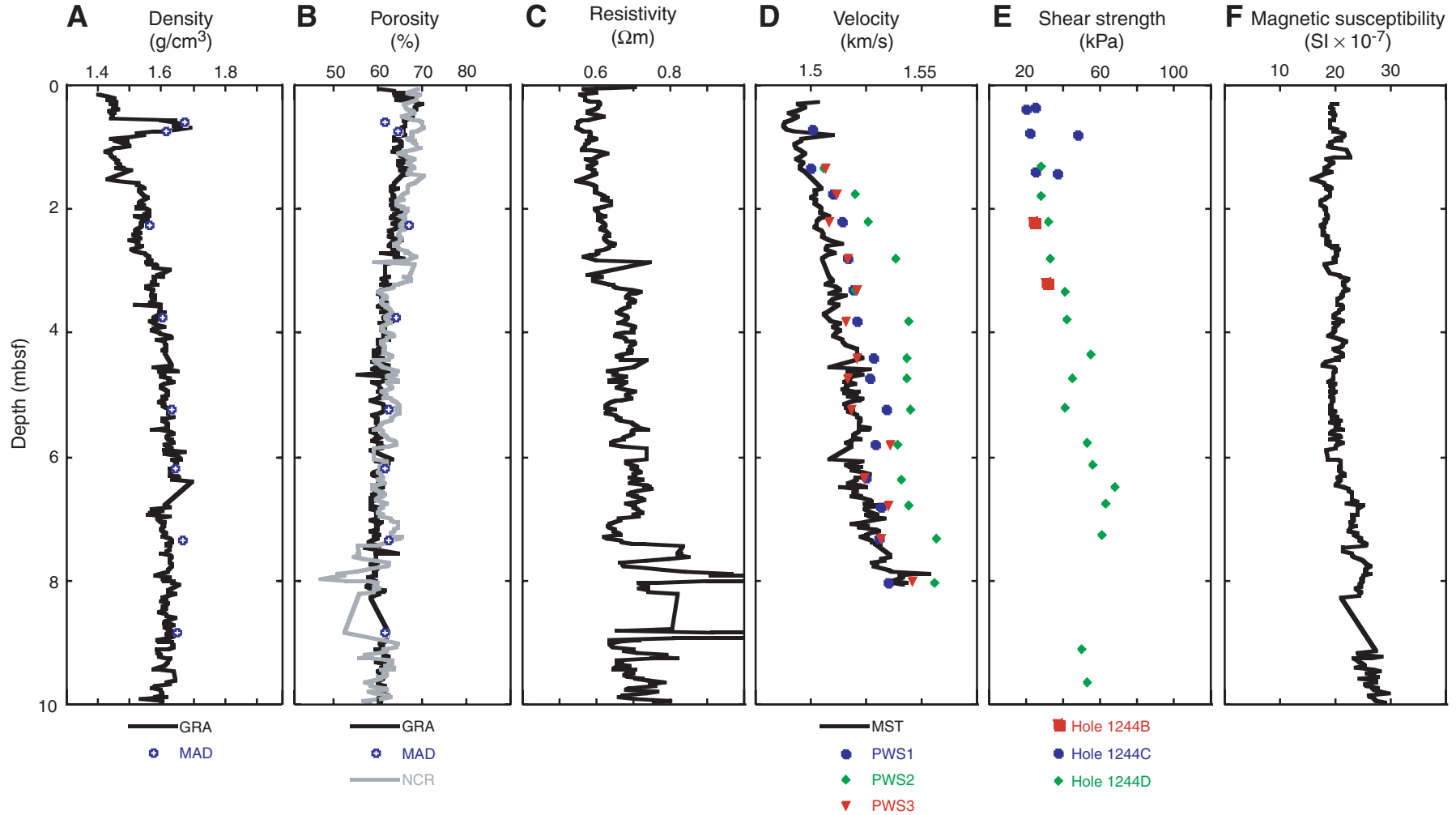
Figure F5. Physical properties of near-surface sediments at Site 1245. **A.** Bulk density. GRA = gamma ray attenuation, MAD = moisture and density. **B.** Porosity. NCR = noncontact resistivity. **C.** Electrical resistivity (NCR). **D.** *P*-wave velocity using multisensor track (MST) and Hamilton frame. PWS = *P*-wave sensor. **E.** Shear strength. **F.** Magnetic susceptibility.
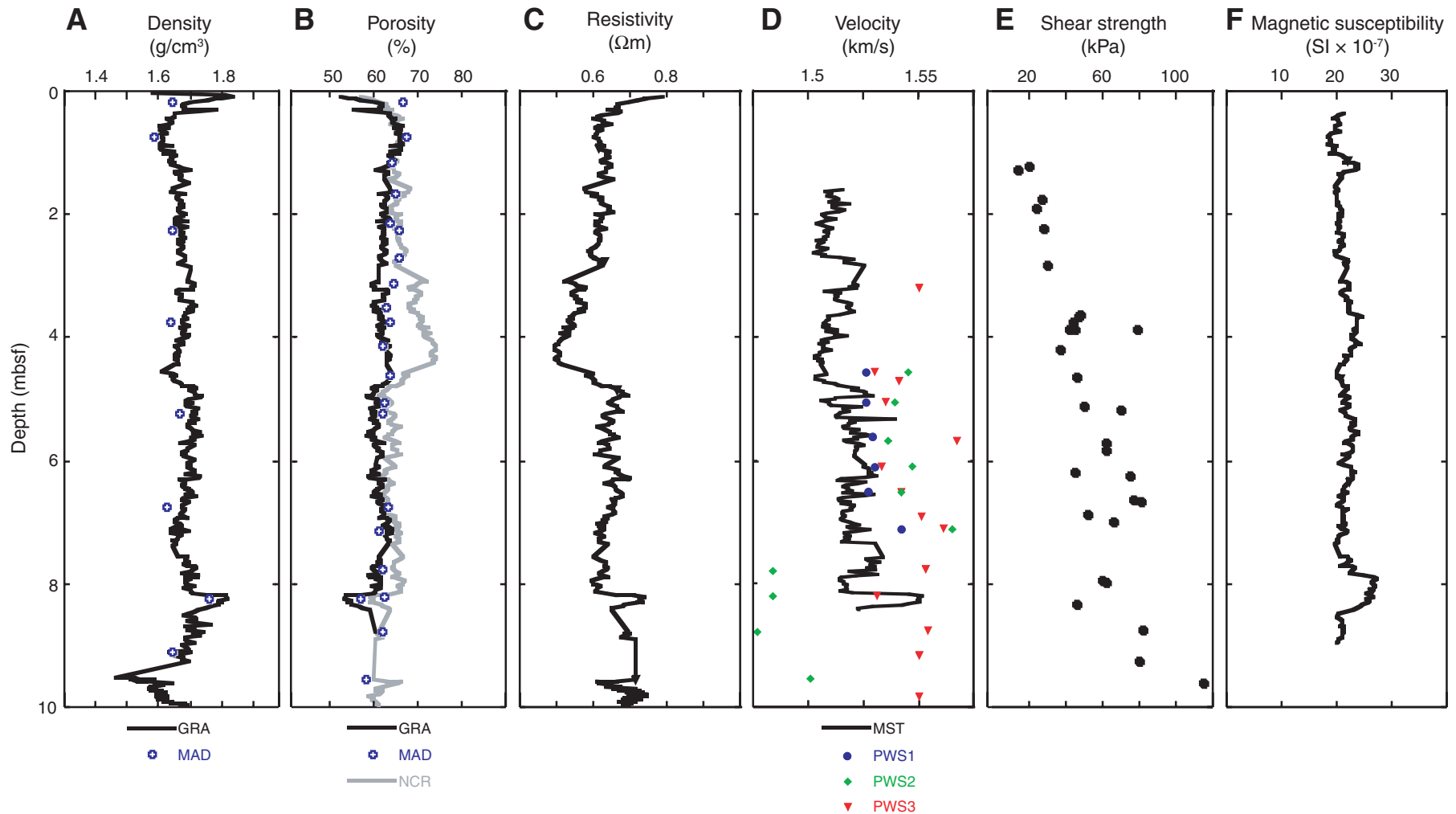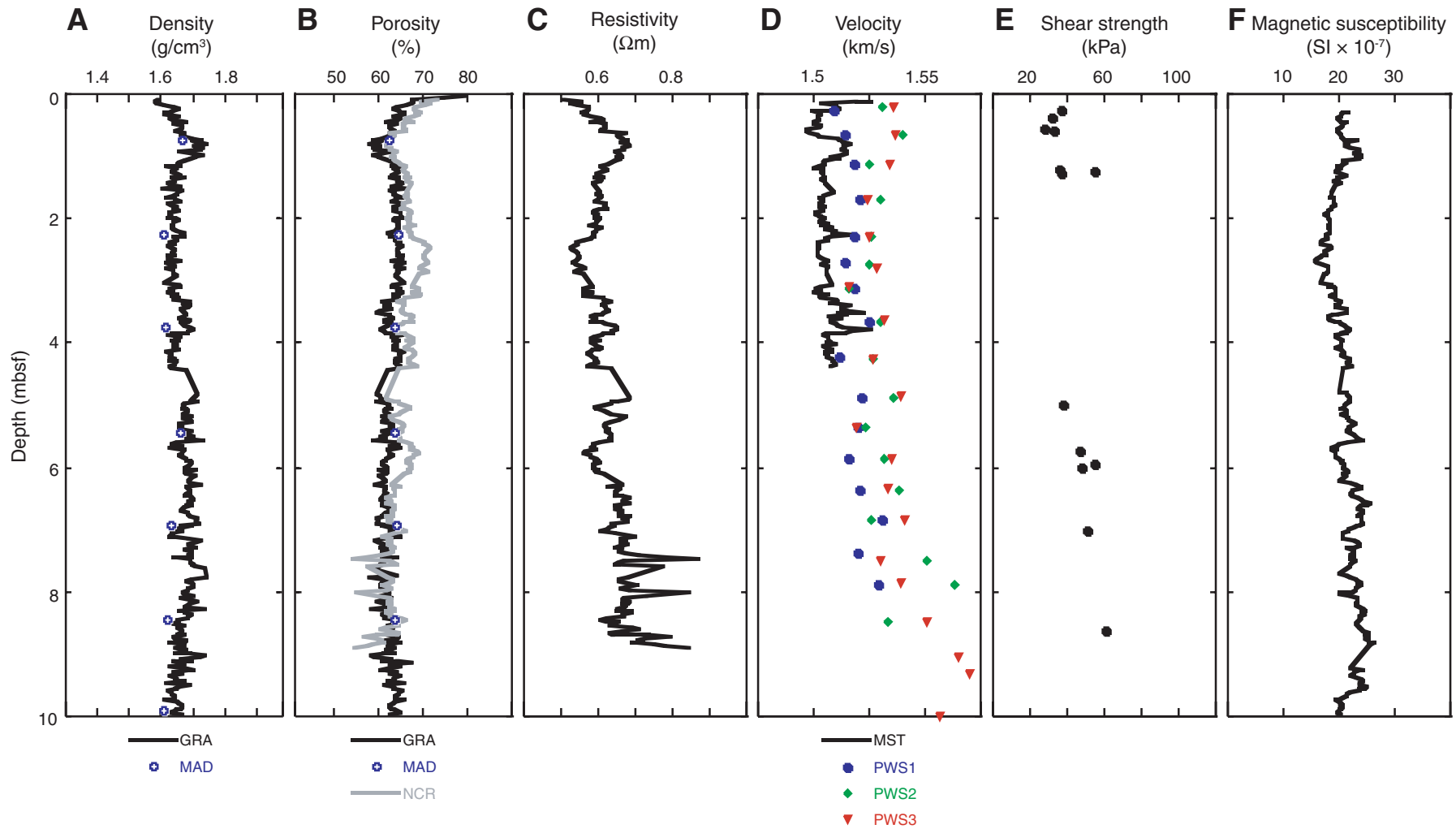
Figure F6. Physical properties of near-surface sediments at Site 1246. **A.** Bulk density. GRA = gamma ray attenuation, MAD = moisture and density. **B.** Porosity. NCR = noncontact resistivity. **C.** Electrical resistivity (NCR). **D.** *P*-wave velocity using multisensor track (MST) and Hamilton frame. PWS = *P*-wave sensor. **E.** Shear strength. **F.** Magnetic susceptibility.

Figure F7. Physical properties of near-surface sediments at Sites 1247 and 1248. **A, C.** Bulk density from gamma ray attenuation (GRA) and moisture and density (MAD). **B, D.** Porosity estimated from GRA, non-contact resistivity (NCR), and MAD data.
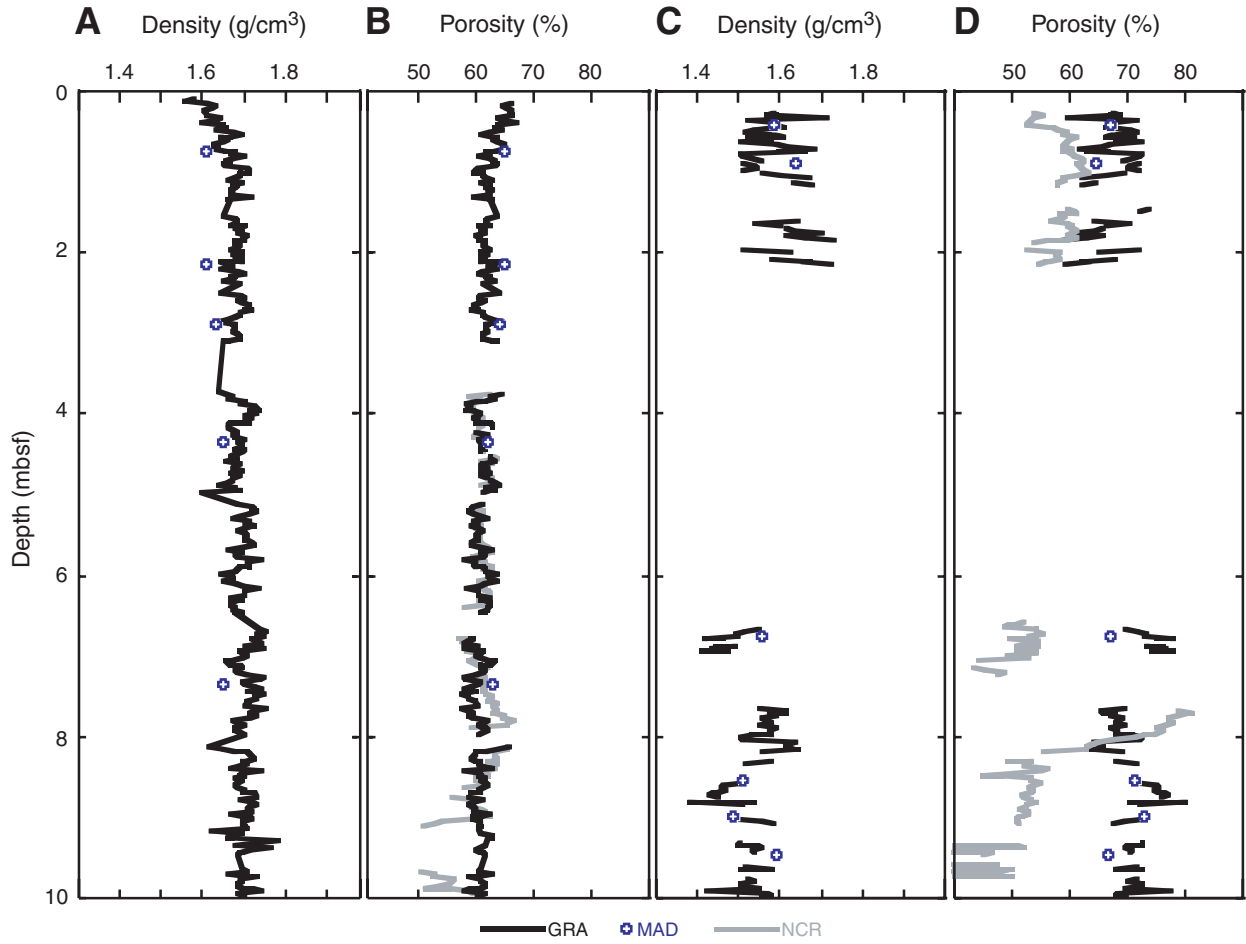
Figure F8. Physical properties of near-surface sediments at Site 1252. **A.** Bulk density from gamma ray attenuation (GRA) and moisture and density (MAD). **B.** Porosity from GRA, noncontact resistivity (NCR), and MAD data. **C.** Electrical resistivity (NCR). **D.** Magnetic susceptibility.
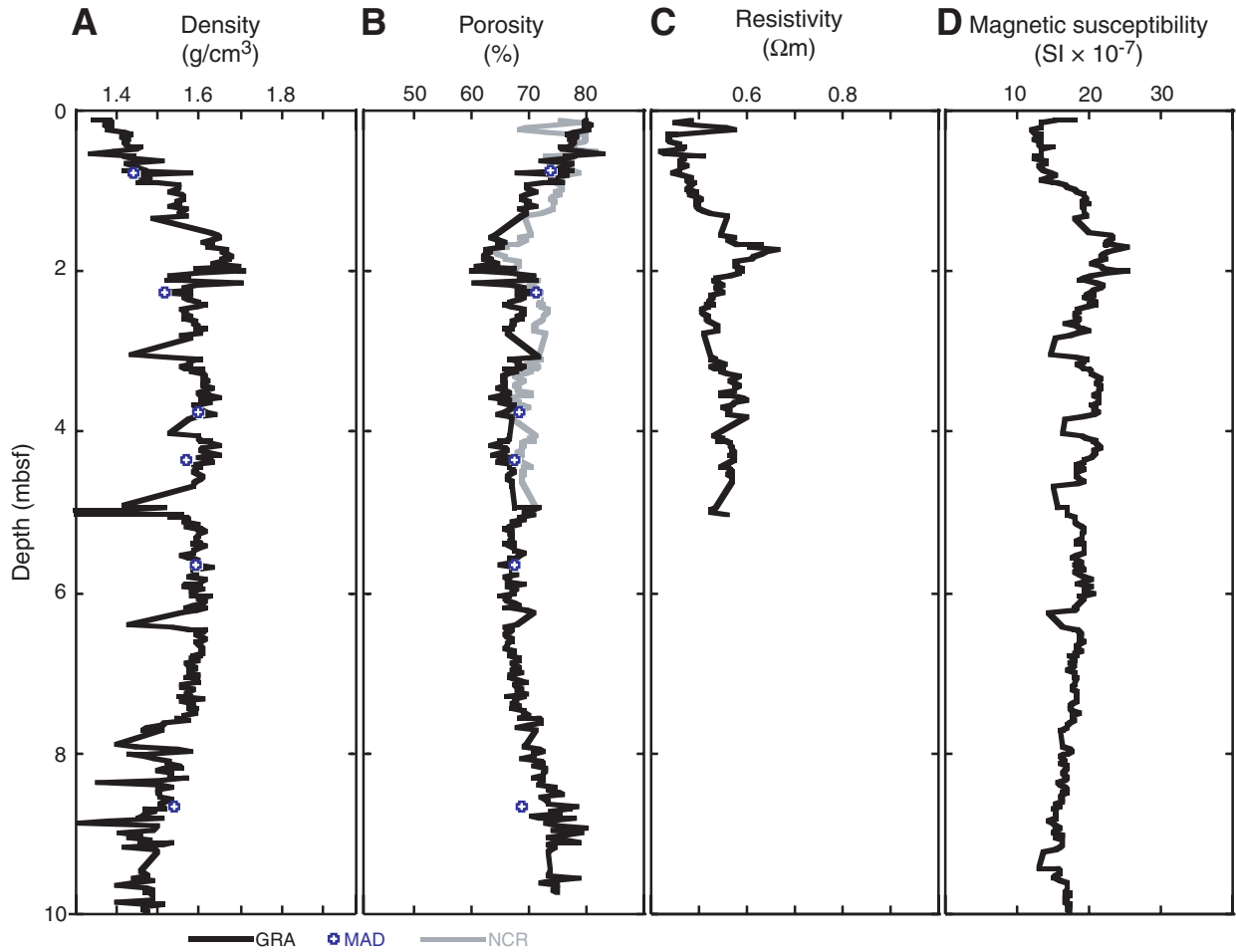
Figure F9. Correlation of porosity and density with velocity and shear strength from all Leg 204 sites. Note that published relations of velocity and porosity do not explain the observed correlation between porosity and velocity for Leg 204 near-surface sediments.
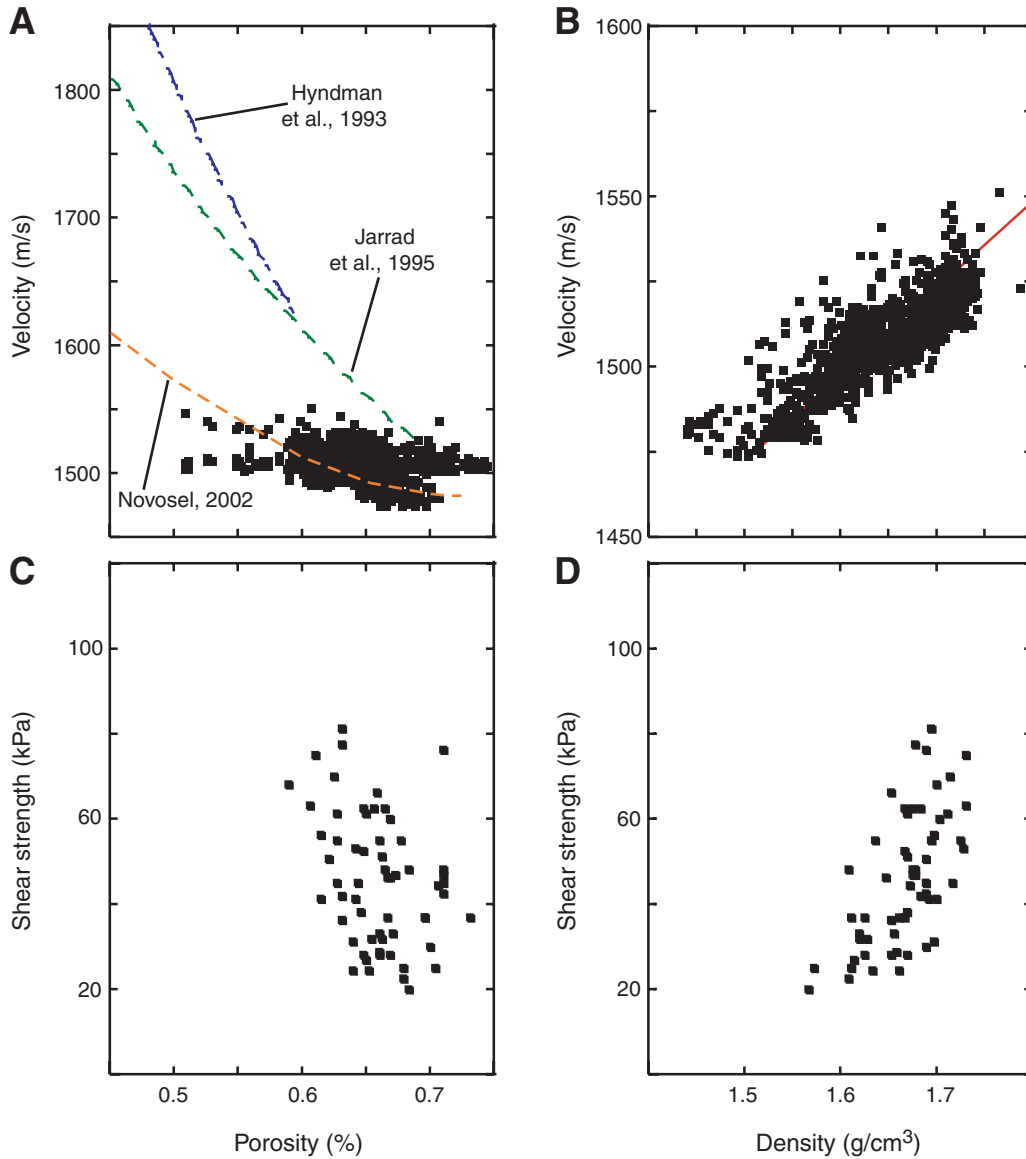
Figure F10. Correlation of velocity with and shear strength. **A.** All data. PWS = *P*-wave sensor, MST = multi-sensor track. **B.** MST velocity values. **C.** PWS-1 velocity values. **D.** PWS-2 s velocity values. **E.** PWS-3 velocity values.
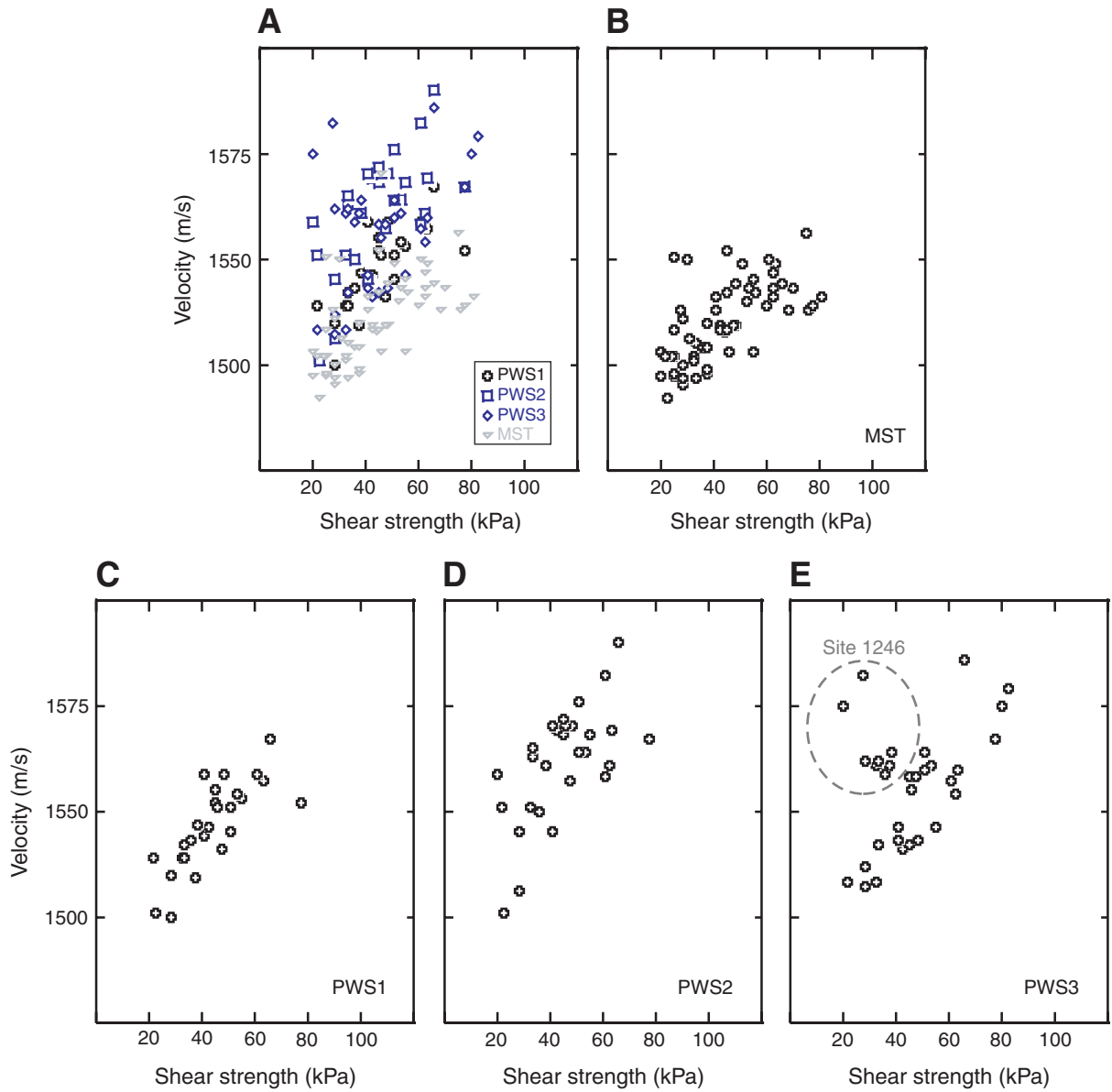
Figure F11. Downcore seismic impedance for Sites 1244, 1245, and 1246 calculated from GRA density and MST velocity.
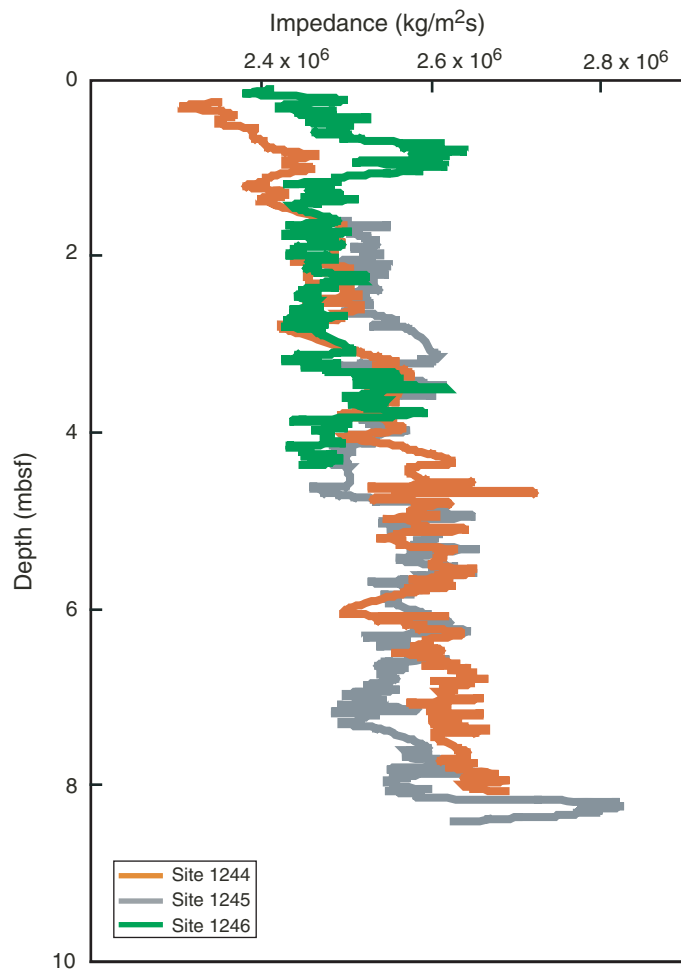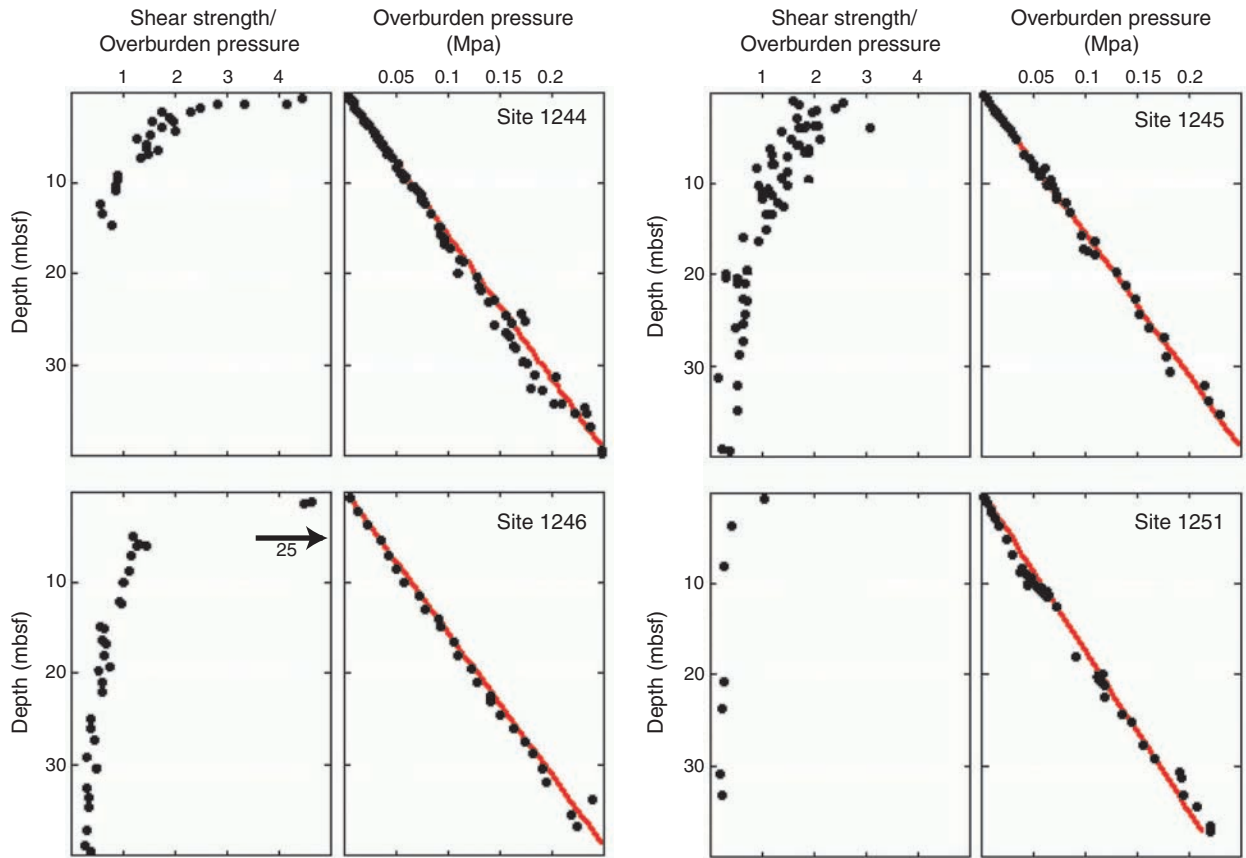
Figure F12. Ratio of shear strength to overburden pressure and calculated overburden pressure at Sites 1244, 1245, 1246, and 1251. Note that at Site 1246, maximum ratio of shear strength to overburden pressure is 25 (off scale).

Figure F13. Downcore porosity (solid circles) for the upper 50 mbsf at Sites 1244, 1245, 1246, 1251, and 1252. The red line is a best-fit using Athy's law for the entire cored section. The blue line is a best-fit using Athy's law for the upper 10 mbsf.
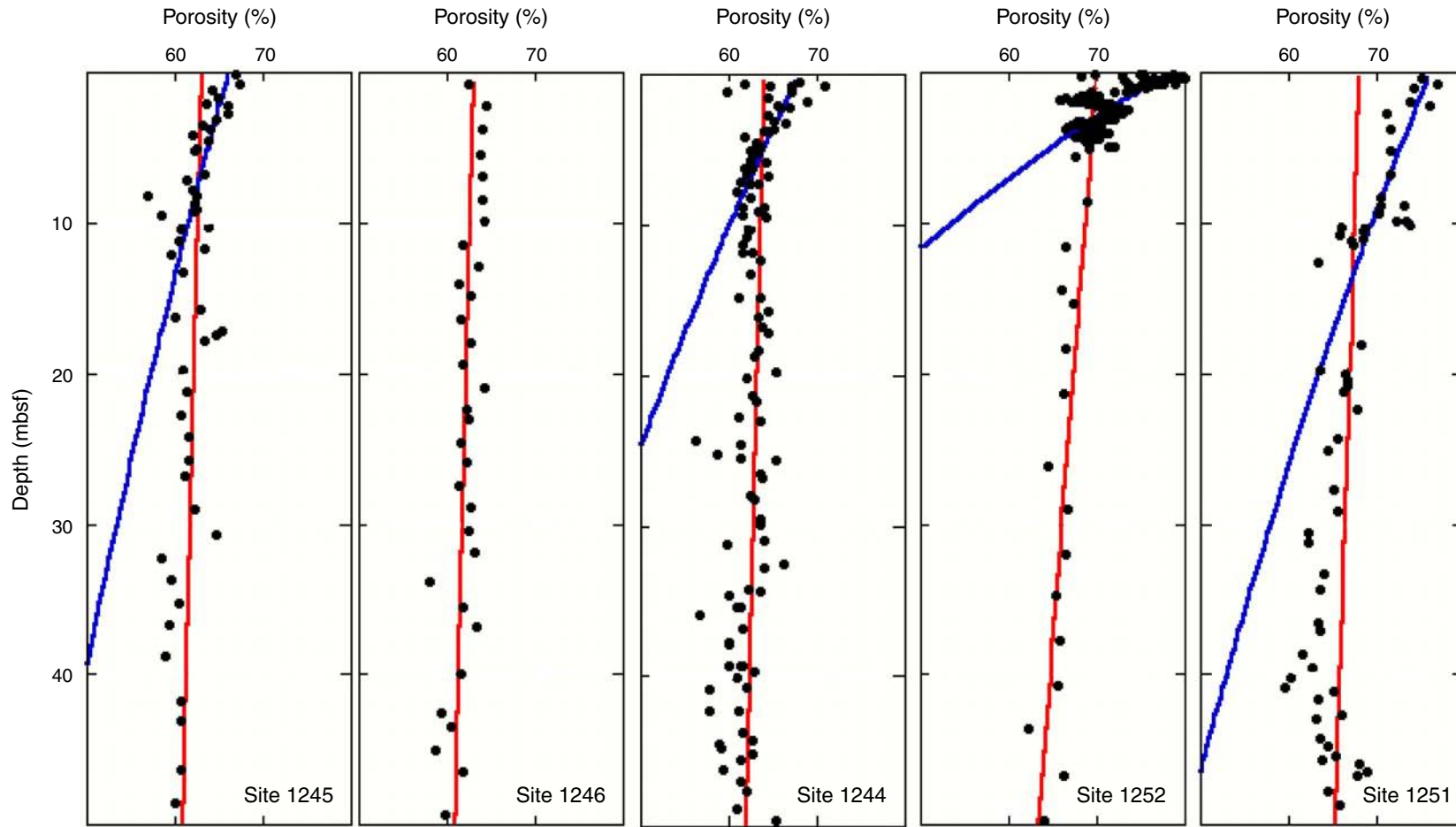
Table T1. Seafloor reflection coefficients.

Depth (mbsf)	Reflection coefficient			Equivalent frequency (Hz)
	Site 1244	Site 1245	Site 1246	
1	0.218	—	0.24	380
2	0.224	0.242	0.237	190
4	0.233	0.245	0.237	95
8	0.25	0.25	—	50

Notes: Equivalent frequencies to resolve a layer of 1.0, 2.0, 4.0, and 8.0 m were calculated using an average velocity of 1500 m/s. — = no data available.

Table T2. Age and average depth of occurrence of biostratigraphic events.

Age (Ma)	Depth (mbsf)								
	Site 1244	Site 1245	Site 1246	Site 1247	Site 1248	Site 1249	Site 1250	Site 1251	Site 1252
0.09	—	—	—	—	—	—	—	17.48	19.36
0.27	76.88	60.96	84.82	37.74	—	24.28	46.32	160	76.35
0.3	86.65	42.68	38.53	39.7	1.19	13	35.86	160	86.04
0.46	86.65	80.47	103.34	59.08	35.5	35.19	46.32	196.5	95.7

Notes: Events determined from microfossil analyses of Su et al. (2003) and Tréhu, Bohrmann, Rack, Torres, et al. (2003). — = no data available.

Table T3. Decay constants and surface porosities.

		Site 1244	Site 1245	Site 1246	Site 1251	Site 1252
All depths	ϕ_0 (%)	63	63	63	68	70
	L (m)	1500	1400	1400	1200	500
Shallow depths only	ϕ_0 (%)	68	66	—	76	79
	L (m)	80	140	—	110	26
	Maximum depth (mbsf)	4–6	4–6	—	10	2

Notes: ϕ_0 = surface porosity, L = decay constant. Values calculated from MAD porosities with Athy's law. — = no data available.